Airborne lidar observations of the 2010 Eyjafjallajökull volcanic ash plume

Franco Marenco,[1] Ben Johnson,[1] Kate Turnbull,[1] Stuart Newman,[1] Jim Haywood,[1] Helen Webster,[2] and Hugo Ricketts[3]

Received 13 June 2011; revised 16 August 2011; accepted 18 August 2011; published 4 November 2011.

[1] Lidar observations of volcanic ash are reported, that have been obtained during six flights of the Facility for Airborne Atmospheric Measurements BAe-146 research aircraft over the United Kingdom and the surrounding seas in May 2010, after the eruption of Eyjafjallajökull. Due to safety restrictions, sampling has only been done in areas where forecasted concentrations were smaller than 2000 $\mu g/m^3$. Aircraft in situ measurements of size-distribution permitted evaluation of a coarse extinction fraction (ranging 0.5–1) and a coarse mode specific extinction (0.6–0.9 m^2/g) for each flight. These quantities were then used to convert the lidar-derived aerosol extinction to ash concentration (with an estimated uncertainty of a factor of two). The data highlight the very variable nature of the ash plume in both time and space, with layers 0.5–3 km deep observed between 2 and 8 km above sea level, and featuring an along-track horizontal extent of 85–550 km. Flights on 14–17 May showed typical concentrations of 300–650 $\mu g/m^3$, and maxima of 800–1900 $\mu g/m^3$ in relatively small high density patches. Column loads for these flights were typically 0.25–0.5 g/m^2 (maxima 0.8–1.3 g/m^2). Relatively small regions characterized by a larger ash content have been selected, and the distribution of ash concentrations and column loadings within them proved rather broad, showing how fractal and patchy the observed ash layers are. A visual comparison of our data set with the "dust RGB" maps from SEVIRI showed a good spatial correlation for the larger ash content days. Moreover, ash prediction maps output from the NAME dispersion model show reasonable agreement with the overall magnitude of the observed concentrations; in some cases, however, there are positional errors in the predicted plume location, due to uncertainties in the eruption source details, driving meteorology, and in the model itself.

Citation: Marenco, F., B. Johnson, K. Turnbull, S. Newman, J. Haywood, H. Webster, and H. Ricketts (2011), Airborne lidar observations of the 2010 Eyjafjallajökull volcanic ash plume, *J. Geophys. Res.*, *116*, D00U05, doi:10.1029/2011JD016396.

1. Introduction

[2] Volcanic ash received a great deal of public attention when an unprecedented disruption of air traffic occurred following the eruption of the Eyjafjallajökull, Iceland, in April and May 2010 [*Gertisser*, 2010]. Volcanic emissions to the atmosphere typically include gases such as water vapor, CO_2, SO_2, H_2S, CH_4, CO, HCl, HF, HBr, and NO_x [*Hobbs et al.*, 1991; *Hunton et al.*, 2005]; sulphate-rich accumulation mode secondary particles, partly neutralized but mostly acidic; and ash thought to be composed of electrostatically charged glassy particles containing Si, Al, Mg, Fe, K, Ca [*Pieri et al.*, 2002; *Carn et al.*, 2011]. Their study remains quite a difficult task, despite the fact that a range of observational means can be deployed such as ground-based in situ probes, radar and lidar remote sensing, satellite imagery, and instrumented aircraft. Aircraft observations prior to this eruption have for instance been reported by *Hobbs et al.* [1991], *Pieri et al.* [2002], *Hunton et al.* [2005], *Rose et al.* [2006], *Oppenheimer et al.* [2010], *Carn et al.* [2011], and references therein. A good overview of satellite applications is given by *Thomas and Watson* [2010] and *Prata et al.* [2010], whereas ground-based in situ and remote-sensing observations are described, e.g., by *Gauthier and Le Cloarec* [1998], *Watson and Oppenheimer* [2001], *Allen et al.* [2006], *Zerefos et al.* [2006], and *Hoffmann et al.* [2010].

[3] The response of the aviation industry to volcanic events is affected by large uncertainty in the exact nature of potential hazards [*Guffanti et al.*, 2010]. When volcanic eruptions occur, guidance on the dispersed ash is provided to aviation authorities by the Volcanic Ash Advisory Centres (VAAC). The Met Office, acting as London VAAC, is responsible for volcanoes in the Northeastern Atlantic, and as such it has issued daily forecasts of volcanic ash concentration in response to 2010 eruption. Additionally, observational instrumentation was deployed in the United

[1]Observational Based Research, Met Office, Exeter, UK.
[2]Atmospheric Dispersion, Met Office, Exeter, UK.
[3]Centre for Atmospheric Science, University of Manchester, Manchester, UK.

Kingdom, including ground-based lidars [*Marenco and Hogan*, 2011; R. J. Hogan et al., Lidar and Sun-photometer retrievals of ash particle size and mass concentration from the Eyjafjallajökull volcano, manuscript in preparation, 2011], balloon-borne in situ probes [*Harrison et al.*, 2010], and the United Kingdom's Facility for Airborne Atmospheric Measurements (FAAM, http://www.faam.ac.uk/) BAe146-301 research aircraft, discussed here. Similar deployments occurred across Europe [see, e.g., *Mona et al.*, 2010; *Ansmann et al.*, 2010; *Flentje et al.*, 2010; *Pietruczuk et al.*, 2010; *Schumann et al.*, 2011; *Bukowiecki et al.*, 2011; P. Chazette et al., Eyjafjallajökull ash concentrations derived from both lidar and modeling, submitted to *Journal of Geophysical Research*, 2011]. Satellite-based research has been done by *Clarisse et al.* [2010], *Stohl et al.* [2011], P. N. Francis et al. (Retrieval of physical properties of volcanic ash using Meteosat: A case study from the 2010 Eyjafjallajökull eruption, submitted to *Journal of Geophysical Research*, 2011), and S. C. Millington et al. (Simulated SEVIRI volcanic ash imagery, submitted to *Journal of Geophysical Research*, 2011), whereas near-source aerosol size-distributions were obtained by *Ilyinskaya et al.* [2011].

[4] Following this eruption, air space containing volcanic ash has been subdivided as follows by the civil aviation authorities: areas of high contamination, for ash concentrations larger than 4000 $\mu g/m^3$ (formerly called no-fly zones); areas of medium contamination, for ash concentrations 2000–4000 $\mu g/m^3$ (formerly limited time zones); and areas of low contamination, for ash concentrations 200–2000 $\mu g/m^3$ (formerly enhanced procedures zones) [*European Union*, 2010; *International Civil Aviation Organization*, 2010]. Forecasts for the London VAAC are provided via the Numerical Atmospheric dispersion Modeling Environment (NAME) [*Jones et al.*, 2007], a Lagrangian model with the driving meteorology provided by the Met Office numerical weather prediction Unified Model. Uncertainties in the model predictions arise due to incomplete knowledge of the source emission flux, vertical profile and near-source fallout, the particle size-distribution for ash surviving near source fallout, and the relationship between model predicted mean concentrations over large volumes and localized unresolved peaks, as well as uncertainties on the forecast underlying meteorological fields. Several processes relevant to ash transport are also parameterized (e.g., sub-scale horizontal and vertical diffusion, sedimentation, wet deposition). Volcanic ash predictions have therefore to be supplemented with observations; the latter are also useful for validating the predicted concentrations and potentially assessing model improvements [see, e.g., *Dacre et al.*, 2011; *Devenish et al.*, 2011; A. L. M. Grant et al., Horizontal and vertical structure of the Eyjafjallajökull ash cloud over the UK, a comparison of airborne lidar observations and simulations, manuscript in preparation, 2011; H. N. Webster et al., A comparison of atmospheric dispersion model predictions with observations of SO_2 and sulphate aerosol from volcanic eruptions, submitted to *Journal of Geophysical Research*, 2011; N. I. Kristiansen et al., Performance assessment of a volcanic ash transport model mini-ensemble used for inverse modeling of the Eyjafjallajökull eruption, submitted to *Journal of Geophysical Research*, 2011; B. Devenish et al., Sensitivity analysis of dispersion modeling of volcanic ash from Eyjafjallajökull in May 2010, submitted to *Journal of Geophysical Research*, 2011]. As an example, relatively thin and stable patches of concentrated ash were observed during this eruption, whereas due to the above uncertainties NAME generally predicted a plume up to four times deeper.

[5] At the time of the eruption, the FAAM BAe-146 aircraft was tasked with monitoring the skies over the United Kingdom and the surrounding seas. The principal probe that was used to map the volcanic ash layers was the on-board lidar, operating in the near ultraviolet; we present the data interpretation scheme and results in this paper. Infrared brightness temperature spectra between 3.3 and 18 μm were also measured using the Airborne Research Interferometer Evaluation System (ARIES), and upwelling irradiances in the visible and infrared were recorded using broadband radiometers. Both types of radiative measurements showed a good correlation with the lidar observations, and the profiles derived from the latter permitted radiometric closure in radiative transfer computations (S. Newman et al., A case study of airborne observations of volcanic ash from the Eyjafjallajökull eruption: 2, submitted to *Journal of Geophysical Research*, 2011). The combination of the lidar with passive radiometric measurements therefore offers a data set for the validation of satellite volcanic ash retrievals, as demonstrated in the above reference. Other probes on the aircraft provided in situ observations. Size-distributions in the 0.1–50 μm range were measured with two wing-mounted optical particle counters, a Cloud and Aerosol Spectrometer (CAS) and a Passive Cavity Aerosol Spectrometer Probe (PCASP). Single-particle imaging in the 45–900 μm range was provided by a 15 μm resolution Cloud Imaging Probe (CIP15). Aerosol scattering coefficients were determined using a TSI 3563 three-wavelength nephelometer; and the concentrations of SO_2, O_3 and CO were determined using trace gas analyzers (B. Johnson, In situ observations of volcanic ash clouds from the FAAM aircraft during the eruption of Eyjafjallajökull in 2010, submitted to *Journal of Geophysical Research*, 2011; K. Turnbull et al., A case study of airborne observations of volcanic ash from the Eyjafjallajökull eruption: 1, submitted to *Journal of Geophysical Research*, 2011). In situ sampling has been limited during this campaign, since the FAAM BAe-146 was subject to the same limitations as other jet engine aircraft. However, the size-distributions provided valuable microphysical information that will be used here in conjunction with the lidar observations. Finally, vertical profiles of meteorological parameters have also been obtained using dropsondes launched from the FAAM BAe-146.

2. Lidar Observations

[6] The lidar, an ALS450 manufactured by Leosphere, is an elastic backscattering system with daytime capability, suitable for aerosol and thin cloud observations, and featuring a depolarization channel. This commercially available lidar is light, compact, eye-safe and simple to operate. It was designed to offer robust performance for ground-based applications and it requires very limited maintenance. Its operational wavelength is 355 nm, and on the FAAM BAe-146 aircraft it is mounted in a nadir-viewing geometry. Measurements were taken with a vertical resolution of 1.5 m and an integration time of 2 s, but vertical smoothing

Table 1. Summary of the Research Flights

Flight	Date	Takeoff	Landing	Area	Main Observations
B521	20 Apr	11:24	17:02	Scotland, North Channel	No significant ash
B522	21 Apr	10:20	11:35	S. Scotland, N. England	No significant ash
B523	21 Apr	13:40	18:56	Orkney and Faeroe Islands	No significant ash
B524	22 Apr	10:09	15:28	North Sea	No significant ash
B525	22 Apr	16:35	17:22	S. Scotland, N. England	No significant ash
B526	4 May	10:04	15:51	Irish Sea	Two aerosols (ash and non-ash); patches; small concentration
B527	5 May	09:11	15:07	Scotland; Irish and North Seas	Ash 2.5–5.5 km
B528	14 May	10:07	19:17	Scotland and N. England (double flight)	Ash 5.5–8 km, occasional cirrus
B529	16 May	12:55	18:10	Scotland and N. England	Main ash plume 55–56°N
B530	17 May	11:26	16:58	Irish and North Seas	Main ash plume over North Sea (1–2°E)
B531	18 May	09:44	14:54	North Sea	Ash in small concentration

with a running average and additional integration were applied during the post-processing in order to reduce the signal-to-noise ratio. Data presented here thus have a vertical resolution of 45 m and an integration time of 1 min; as the aircraft travels at a ground speed of 120–180 m/s (typical at an altitude of 6–10,000 m), the latter translates into a 7–11 km footprint. Full overlap of the receiver field-of-view with the emitted beam is achieved at a range of 300 m, and only data beyond this point will be considered here.

[7] Twelve research flights, for a total of 53 flying hours, were carried out between 20 April and 18 May 2010, as detailed in Table 1 (including a double flight on 14 May). As our aircraft was subject to the same safety limitations of civil airlines, only areas with forecasted ash concentrations less than 2000 $\mu g/m^3$ could be targeted. Our focus in this article will be on the May flights (six flights and 1890 vertical profiles), as only dilute concentrations of volcanic aerosols were observed at the sampled locations during the early flights (<100 $\mu g/m^3$ (see Johnson et al., submitted manuscript, 2011). Note that Coordinated Universal Time (UTC) is used throughout this paper.

3. Interpretation of the Lidar Returns

[8] Prior to a quantitative data analysis, all individual 1 min lidar profiles have been individually inspected to identify molecular and cloud layers. Molecular layers have been identified where the signal fits a Rayleigh scattering profile, computed accounting for both scattering and extinction. Cloud tops have been identified by the sudden increase of signal intensity by a large amount (often more than an order of magnitude), followed by a strong attenuation of the lidar signal beyond. Every time a cloud top was found, the cloud and everything beyond it has been removed from the data set. Note however that optically thin clouds (cirrus) may be hard to distinguish from aerosol layers; an additional verification is therefore made using the nearest relative humidity profile from either the aircraft ascent or descent, or a dropsonde. Lidar profiles taken during aircraft turns (off nadir angle larger than 10°) have also been removed from the data set, as the slant path correction has been found to be sensitive to the aircraft roll angle as it rapidly varies.

[9] The processing of the lidar profiles is made by a double iteration: in the first iteration, the lidar ratio (extinction-to-backscatter ratio) is determined. A subset of the lidar profiles, representative of the six flights, is selected where the aerosol layer is surrounded by layers both directly above and directly below where molecular scattering appears dominant. The latter allows determination of the optical depth of the aerosol layer circumscribed by molecular layers, as in the work by *Di Girolamo et al.* [1994]: this constraint permits inference of a lidar ratio (assumed constant with height) representative of the considered layer. Molecular layers were identified by fitting to a Rayleigh backscattering and extinction profiles, and the fits were individually verified by visual inspection. Although the presence of aerosols active at the lidar wavelength in the free troposphere cannot be completely ruled out, we believe the normalization to a molecular profile to be reasonable given that during that period infrared lidars at Cardington and Chilbolton, United Kingdom, showed no signal above the volcanic layers or between the latter and the boundary layer. *Young* [1995] evaluated a typical backscattering coefficient in free tropospheric aerosols to be 1–5% of molecular backscattering at a wavelength of 532 nm; in our case, the 355 nm wavelength ensures an even larger dominance of molecular backscattering (five times larger according to the fourth-power dependence upon frequency). If however, despite all precautions, some aerosols were to be indeed present at the normalization heights, a bias could result as investigated by *Marenco and Hogan* [2011]; generally this would lead to an overestimated lidar ratio.

[10] The lidar ratios determined in this manner were found to have a mean of 61 sr, a standard deviation of 13 sr, and a median of 59 sr (637 vertical profiles); their distribution has been found to be near to Gaussian, with little variation from flight to flight. As a result, a lidar ratio of 60 sr has been chosen in the present article as representative of all the observed aerosol layers, and has thus been extrapolated for use with aerosols not circumscribed by two molecular layers. This estimate of the lidar ratio is in agreement with the findings from ground-based Raman lidars: e.g., *Ansmann et al.* [2010] found 55–60 sr, whereas *Mona et al.* [2011] found 40–80 sr depending on the humidity content of the ash layer.

[11] Using the lidar ratio determined above, a second iteration on the raw lidar measurements has been done, and the whole data set has been inverted into aerosol extinction profiles using the Fernald-Klett algorithm [*Fernald*, 1984; *Klett*, 1985]. Figure 1 displays the resulting estimate of the aerosol extinction coefficient for each of the six flights, as a function of time and height. Accounting for the assumptions made, we estimate an uncertainty of ±30% for these

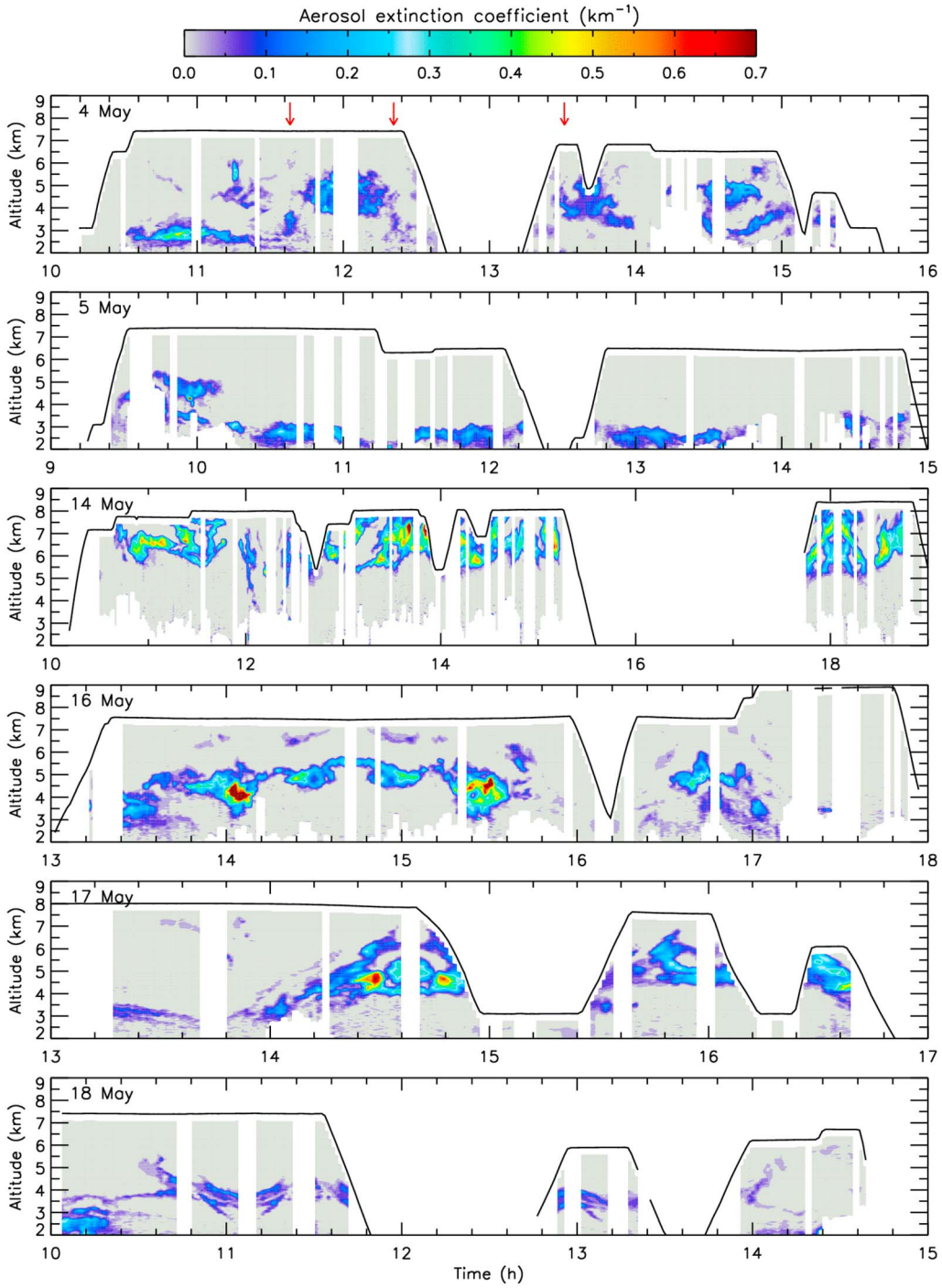

Figure 1. Aerosol extinction coefficient estimated from backscatter lidar observations, for the indicated dates and times. Gaps indicate missing data, due either to rejection of whole profiles or rejection of the portion of profiles affected by clouds (see text). The solid line depicts the FAAM BAe-146 aircraft altitude. The red arrows in the 4 May panel indicate the overpasses of Aberystwyth.

retrievals. Significant variability in the structure of the aerosol plume is evident, with layers at altitudes between 2 and 8 km, leading to aerosol extinction coefficients up to 1.2 km^{-1} and aerosol optical depths (AOD) up to 0.85. The plots show rather different magnitudes of the aerosol extinction coefficient for each flight, with flights on 14–17 May showing a clearly larger aerosol content than the flights on 4, 5 and 18 May. Noteworthy are the highly concentrated small areas with a large aerosol extinction on 16 and 17 May. Symmetrical features result from reciprocal turns of the aircraft, with a repeated overpass over the same features.

[12] On 4 May, the FAAM BAe-146 aircraft made three overpasses of the FGAM Flight Ozone and Aerosol Lidar in

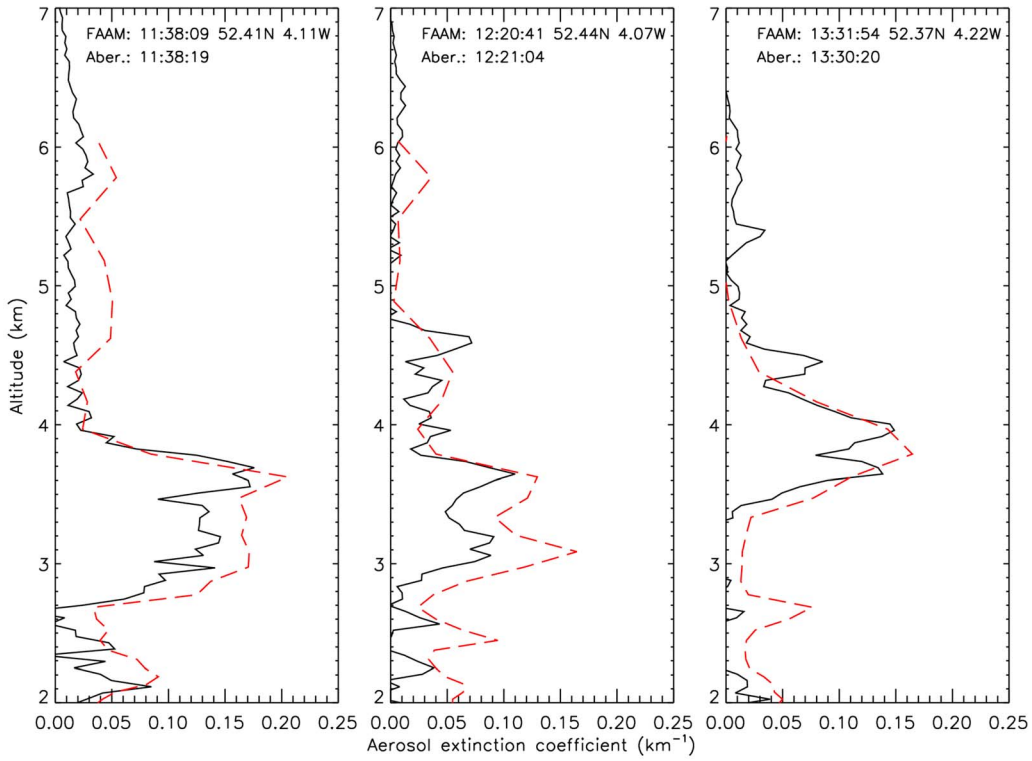

Figure 2. Nearly simultaneous aerosol extinction coefficient profiles, determined from the lidar on-board the FAAM BAe-146 aircraft and the ground-based lidar at Aberystwyth (52.4°N, 4.0°W) on 4 May. Integration time is 1 min for the FAAM lidar and 10 min for the Aberystwyth lidar. FAAM lidar: black solid line; Aberystwyth lidar: red dashed line.

Aberystwyth, which also operates at the 355 nm wavelength; the time of these overpasses is marked with a red arrow at the top of Figure 1. FGAM stands for Facility for Ground based Atmospheric Measurements, part of the National Centre for Atmospheric Science (NCAS). The overpasses present an opportunity to intercompare the measurements taken by the two systems, both retrieved with an identical lidar ratio. Nearly simultaneous and nearly co-located vertical profiles from both systems are displayed in Figure 2; we see that while the agreement is generally good, there are significant differences, as might be expected in aerosols exhibiting a high degree of spatial and temporal variability. Both lidars place the main aerosol layer at the same altitude and the magnitude of the extinction coefficient is within 25% for the first and the third plot (but is of the order of 50% in the lower half of the second plot). The two systems show a slightly different layering of the atmosphere, though. We believe that these differences may be in great part ascribed to the different integration times used (1 min for the airborne lidar, 10 min for the ground-based lidar) and to the non-exact co-location of the two systems in a quite inhomogeneous atmosphere (the airborne lidar having a 7–11 km footprint).

[13] In the lidar returns, we distinguish layers containing volcanic ash from other aerosols using depolarization, a quantity considered a good tracer for volcanic ash and mineral dust [see *Freudenthaler et al.*, 2009; *Hoffmann et al.*, 2010; *Ansmann et al.*, 2010]. Unfortunately we have found that, as the aircraft altitude increases and the operating temperature rapidly drops below a given threshold, a temperature-dependent effect is seen in the depolarization channel. As a consequence of this unexpected behavior, we are unable to use depolarization in a quantitative manner as in the work of *Marenco and Hogan* [2011]. In the future, we plan to better characterize the lidar system and stabilize its operating environmental conditions. For the present campaign we do not show depolarization results; the qualitative information of whether an aerosol depolarizes light or not is however still available, and is used to give us extra confidence that the observed aerosols contain volcanic ash. The identification of the aerosols is also justified by the examination of the synoptic analysis, which indicates an air flow from Iceland, and by a comparison with satellite imagery; furthermore, size-distributions obtained in situ display a dominant concentration in the coarse particle mode (see next section).

4. Estimates of Ash Concentration

[14] An estimate of the ash mass concentration from the lidar measurements is highly desirable, as this quantity was forecast by the NAME dispersion model, and is required for aviation safety regulations. The lidar returns constitute a far more spatially extensive data set than the in situ probes on the FAAM BAe-146 aircraft can offer, thanks to its profiling capability. Although not directly measured by the lidar, concentration can be estimated by combining the lidar measurements with size-distribution information derived

Table 2. Per-Flight Estimate of Microphysical Parameters at 355 nm, Deduced From the Observed Size Distributions[a]

	Mie		Irregular	
Date	f_c	K_{ext} (m^2/g)	f_c	K_{ext} (m^2/g)
4 May	0.45	0.70	0.52	0.92
5 May	0.65	0.47	0.72	0.65
14 May	0.96	0.45	0.97	0.62
16 May	0.72	0.62	0.78	0.82
17 May	0.77	0.53	0.82	0.72
18 May	0.69	0.55	0.75	0.74

[a]Shown are coarse particle extinction fraction (f_c) and coarse particle specific extinction (K_{ext}), computed for the spherical (Mie) and irregular ash particle shapes. The values for irregular particles are used throughout this work, and the Mie scattering values are given for a comparison.

from the in situ probes on-board the aircraft. The lidar and the in situ probes have therefore proved to be complementary to a large degree.

[15] Size-distributions have been measured aboard the FAAM BAe-146 aircraft with a 10 s integration time, using the PCASP and CAS optical particle counters, covering respectively the size ranges 0.1–3 μm and 0.6–50 μm (volume-equivalent diameter) (Johnson et al., submitted manuscript, 2011). The fact that particles were not detected by the CIP15 when flying in the ash layers gives us confidence on the fact that we are not missing larger particle sizes. The lidar-derived aerosol extinction cannot be attributed to volcanic ash only, since the size-distributions are found bimodal and show both fine and coarse modes; it is the latter only that we ascribe to volcanic ash. The fine fraction could, for example, be attributed to secondary aerosols originating from gases, such as SO_2, also emitted by the volcano (e.g., sulphuric acid or ammonium sulphate). *Schumann et al.* [2011], for instance, show that particles with a diameter smaller than ~0.5 μm are prevalently ascribed to secondaries, whereas larger particles are mainly silicates, and internal mixtures of silicates and ammonium sulphate. In our data set, the minimum of the bimodal size-distributions has been found at 0.6 μm, and this value has thus been considered being the cutoff between the two modes.

[16] Scattering data from the optical particle counters has been interpreted by assuming a spherical shape for the fine mode, with a refractive index $n_f = 1.43$ (typical for sulphuric acid). The assumed coarse mode density is $\rho_c = 2.3$ g/cm^3 for consistency with the ash properties specified in the NAME dispersion model, and the refractive index is assumed to be $n_c = 1.52 - 0.0015 \cdot i$ based on the mineral dust data set of *Balkanski et al.* [2007] with a medium level of hematite. For the coarse mode (ash), two interpretation schemes have been used, assuming either spheres or irregular particles. For the spherical case a Mie scattering code is used, whereas for the irregular case a mixture of hexagonal columns and polyhedral crystals is assumed, and resolved using a ray tracing method with diffraction at facets [*Osborne et al.*, 2011; Johnson et al., submitted manuscript, 2011].

[17] The ash mass is dominated by particles in the size range 1–10 μm, with a maximum observed diameter ranging 20–35 μm, and is fairly well represented by a lognormal. Although we are confident in qualifying the observed aerosol layers as containing ash, when making quantitative estimates we must ensure that we remove the contribution to scattering due to the fine fraction. This can be achieved by multiplying the lidar-derived aerosol extinction coefficient α by the extinction fraction that is ascribed to coarse particles, f_c. Volcanic ash mass concentration estimates can then be computed by applying the coarse mode specific extinction, K_{ext}. Estimates of f_c and K_{ext} have been computed from the size-distribution by light scattering computations, for each flight and for each of the two ash particle shapes mentioned above: see Table 2 (Johnson et al., submitted manuscript, 2011). Note that f_c is different from the coarse particles mass fraction, as scattering by a large number of small particles tends to be much larger than their mass fraction may suggest.

[18] To better understand which microphysical parameters affect the specific extinction in the coarse mode, we give here an approximate formula derived from basic theory [see, e.g., *Van de Hulst*, 1957], mainly for the purpose of qualitative considerations. In the geometrical optics limit, $K_{ext} \sim 3/(2\rho_c R_e)$, where R_e is the effective radius defined as $R_e = 3V/4A$, and V and A are the volume and projected area averaged over the size-distribution, respectively. The main factors affecting K_{ext} are thus the density and R_e, where the latter is affected by both particle size and shape. For instance irregular particles have a larger projected area compared to equivalent-volume spheres, and thus a larger specific extinction; this is what we observe in Table 2, where specific extinctions obtained for Mie scattering are ~25% smaller than their counterparts computed for irregular particles. For the very large particles in a given size-distribution, therefore, the assumed value for the refractive index does not play a critical role in the determination of the specific extinction; as however the size-distribution itself is derived from an optical particle counter after assumption of a refractive index, this parameter in fact plays an important role too, and not only for the smaller particles. For an example of how the assumed refractive index affects the measured size-distribution see, e.g., Turnbull et al. (submitted manuscript, 2011). In all our light scattering computations, full accountance for particle size, shape and refractive index is made. In what follows, we shall refer to f_c and K_{ext} as computed for the irregular particles case.

[19] We estimate the volcanic ash concentration M as follows:

$$M = \frac{f_c\,\alpha}{K_{ext}}, \tag{1}$$

as displayed in Figure 3, and using the microphysical parameters f_c and K_{ext} for irregular ash particles in Table 2. Not surprisingly, Figure 3 shows many of the same features displayed in Figure 1; volcanic ash concentrations up to almost 2000 μg/m^3 are found, and the very variable nature of the ash concentration is again evident. Flights on 14–17 May, again, show a larger tropospheric ash content, when compared to the remaining three flights, and localized higher ash concentration areas are recorded on 16–17 May. We estimate an overall uncertainty of a factor of two on ash concentration, which has been estimated by accounting the

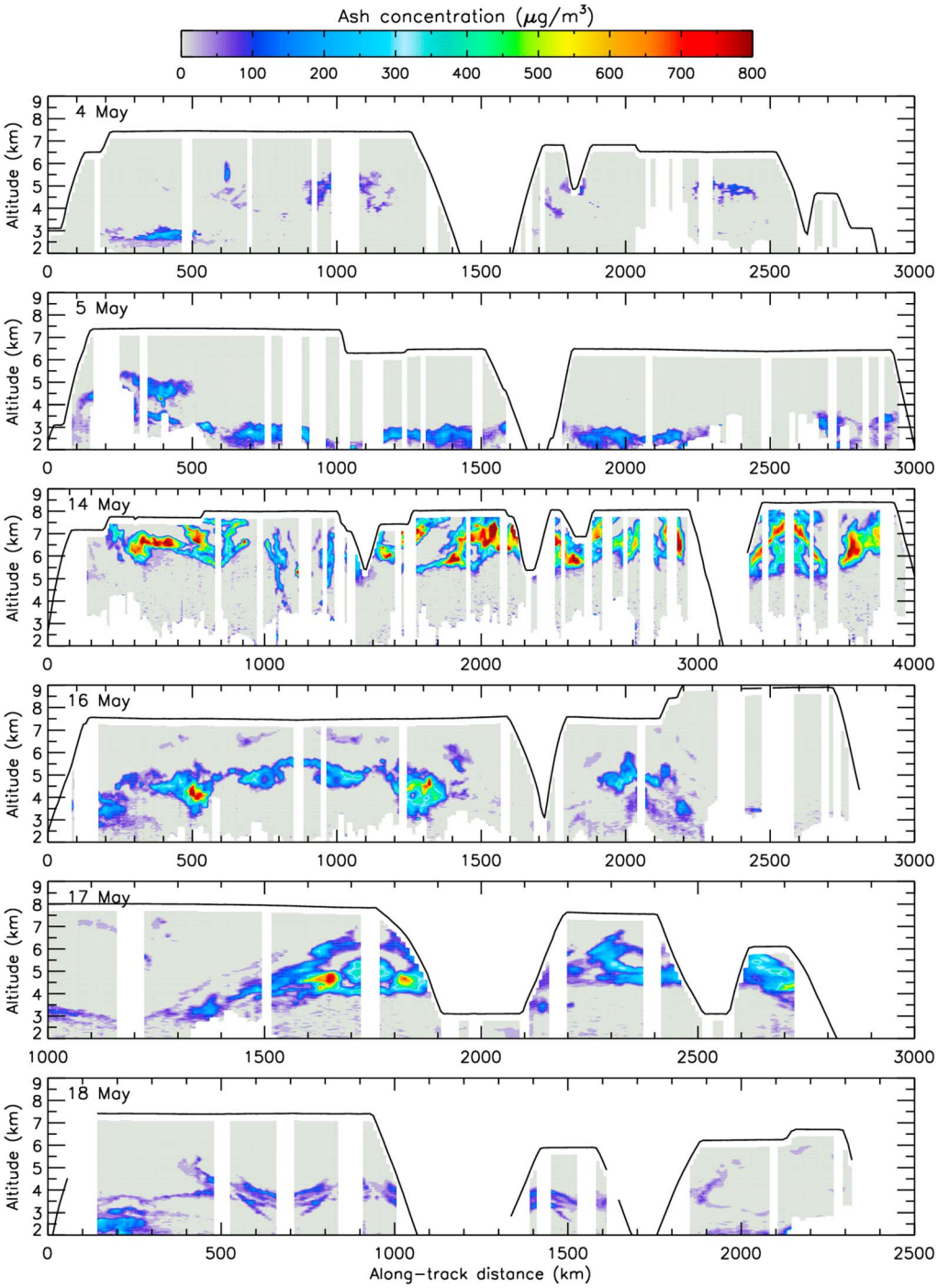

Figure 3. Volcanic ash concentration determined from the lidar, for the indicated dates, assuming the microphysical parameters given in Table 2.

errors of the CAS instrument (sizing accuracy and counting accuracy), the uncertainty on the microphysical model used for ash (particle shape and refractive index), and the uncertainty on ash density: for details on how this uncertainty has been estimated, see Johnson et al., submitted manuscript (2011). In the rest of this work, we shall express our results in terms of mass concentration, as it is the quantity of interest; the reader is advised on the large uncertainty that this choice represents.

[20] The coarse mode extinction fraction exhibits rather similar values for four flights (5, 16, 17 and 18 May). The other two flights deserve a specific discussion of the interpretation of the observations, since several complementary measurements indicate that the observed layers on those days have different properties. On 4 May only small concentrations of aerosol were observed ($\leq$300 μg/m^3), and the fine fraction was more significant than in other flights (see Table 2). Moreover, the aerosol spatial distribution showed

a large inhomogeneity, with patches of non-depolarizing aerosols observed as well as patches of depolarizing aerosols (depolarization being only qualitative, and not shown here). It must be noted that, when the data analysis described in the previous section has been applied, the non-depolarizing layers yielded a lidar ratio similar in magnitude to the depolarizing layers; we therefore cannot base the distinction between ash and non-ash on this quantity. In going from Figure 1 to Figure 3 we have suppressed the non-depolarizing layers, which we ascribe to the fine fraction only and we believe not to contain volcanic ash.

[21] On 14 May, there was evidence of the presence of ice particles within patches of the ash plume. When in situ observations were made, ambient atmospheric humidities approaching saturation were occasionally encountered, whereas at other times during the flight the layers were found dry. The large humidities coincided with peaks in the concentration derived from the CAS probe, and particles with a diameter >30 μm were found. Size-distributions summarizing that day showed larger particles in general than for the other flights; this is also reflected in the value of f_c. Sharp increases in the lidar returns were also encountered at times within the ash plume, indicating the potential presence of cirrus, and as explained earlier the corresponding vertical profiles have been removed from the data set to avoid any mis-interpretation. For this flight the presence of ice internally or externally mixed with volcanic ash cannot be ruled out, and thus an overestimation of ash concentration might be expected at certain times. Large concentrations were generally encountered on this flight, and cirrus contamination cannot be ruled out.

[22] We can use information from infrared brightness temperature spectra obtained with ARIES to detect the signature of species such as ash and ice. A V-shape absorption feature between 8 and 13 μm is characteristic for the presence of mineral aerosols [*DeSouza-Machado et al.*, 2006]; by contrast the signature of ice is very different and the gradient in observed brightness temperature at 10–12 μm is of opposite sign to that of ash [*Gangale et al.*, 2010]. An examination of the ARIES spectra for 14 May suggests that the atmospheric layers below the aircraft are dominated by ash with perhaps some small ice signal. We remind the reader that volcanic ash particles are considered efficient ice nuclei [*Rose et al.*, 2001; *Durant et al.*, 2008; *Bingemer et al.*, 2011], and therefore scattering may be enhanced by ice coating the ash particles even in the case that the identification of a "true" cirrus is difficult.

5. Discussion

[23] From the volcanic ash concentrations described above, the ash column load and peak concentration have been computed for each vertical profile. They have been computed for a variable section of the atmospheric column, defined as follows: the lower boundary is set at 2 km, in order not to include boundary-layer features, or just above cloud top (whichever is higher). The higher boundary is set at the lidar overlap range, 300 m below the aircraft. To avoid comparing profiles encompassing the whole ash layer from base to top with partial profiles, data obtained when the FAAM BAe-146 aircraft is flying below a given threshold altitude (varying between flights) have been omitted in the computation of ash column load and ash peak concentration.

[24] Table 3 summarizes the flights in terms of the following properties: layer height, layer depth, column load, and peak concentration. For the 5, 14, 16 and 17 May data, a 0.1 g/m^2 threshold on column load has been set for computing these overall per-flight values, in order to avoid considering the measurements taken when not overflying the ash plume; values indicated as "typical" are averages of the data for vertical profiles with column load above the threshold. For the 4 and 18 May, since ash concentrations were low, no threshold has been set (all data were used). The layer height has been defined, for each vertical profile, as the weighted average of the ash vertical distribution, and the layer depth as $\sqrt{2}$ × (column load)/(peak concentration). Note that the definition of layer depth can be rather arbitrary; we have however found that a uniform layer with a concentration equal to the peak concentration divided by $\sqrt{2}$, and a depth as defined above, represents the layers well for radiative transfer. Table 4 gives an indication of the horizontal extent of the major ash layers observed during each flight at different altitudes.

[25] From Tables 3 and 4 we see that ash layers extending from 85 to 550 km in the horizontal direction were observed, and were detected in atmospheric layers between 2.3 and 8.1 km at different times. An ash layer height variability of 2–3 km within every flight was found, and the layer depth was typically ~1 km, but was as large as 2–3 km at times. The flight that measured the largest amount of volcanic ash was 14 May, which presented typical and maximum column loadings of 0.55 and 1.3 g/m^2, respectively, and typical and maximum concentrations of 650 and 1900 μg/m^3. In contrast to other cases, during this flight ash was nearly always confined to ~5.5 km and above. On the other hand, the 4 May case represents the other extreme, with typical and maximum column loadings of 0.05 and 0.15 g/m^2 and typical and maximum concentrations of 90 and 300 μg/m^3, respectively. We remind the reader that aerosol sampled on these two flights exhibited rather different properties to the other flights in many respects (section 4). For the flights on 5, 16, 17 and 18 May, intermediate conditions were observed, with column loadings ranging 0.1–0.3 g/m^2 (typical) and 0.2–0.8 g/m^2 (maximum), and peak concentrations ranging 120–300 μg/m^3 (typical) and 350–1000 μg/m^3 (maximum). A comparison with the concentrations obtained directly from the in situ probes is also included in Table 3, but such a comparison is not always straightforward since the FAAM BAe-146 aircraft mostly flew above the plume for lidar remote sensing (our research aircraft being subject to the same limitations as civil airlines), and the two measurements are inherently offset in time and space. It can be seen that both measurements yield comparable results, although as expected the lidar maximum concentrations are systematically higher than the in situ observations as the former samples the whole vertical profile below aircraft, whereas in situ sampling is unlikely to penetrate the three-dimensional regions with the largest concentration.

[26] Our work can be compared to the results by *Schumann et al.* [2011], describing volcanic ash measurements made with the German Aerospace Center (DLR)

Table 3. Per-Flight Estimates, Derived by Lidar, of Minimum and Maximum Ash Layer Height, Typical and Maximum Ash Layer Depth, Typical and Maximum Ash Column Load, Typical and Maximum Ash Columnar Peak Concentration[a]

Date	Layer Height (km)	Layer Depth (km)		Column Load (g/m^2)			Peak Concentration ($\mu g/m^3$)		
		Typ	Max	Typ	Max	In Situ[b]	Typ	Max	In Situ[b]
4 May	2.3–5.5	0.5	1.5	0.05	0.15	0.05	90	300	160
5 May	2.4–4.5	0.9	1.9	0.15	0.4	0.15	250	600 (1100)[c]	580
14 May	5.1–8.1	1.1	2.7	0.55	1.3	0.1–1 (5.5)[d]	650	1900	1400 (4700)[d]
16 May	3.4–5.5	1.2	2.1	0.25	0.8	—	300	1000	130
17 May	3.5–5.6	1.3	2.0	0.3	0.75	0.1–0.7	300	800	510
18 May	2.5–4.9	0.9	1.5	0.1	0.2	0.15	120	350	210

[a]See text.

[b]In situ ash observations derived from the CAS probe (Johnson et al., submitted manuscript, 2011). In situ column loads indicate typical values obtained when the FAAM BAe-146 aircraft profiled through the ash layer. In situ concentrations indicate the maximum concentration encountered during a flight.

[c]On 5 May a single isolated concentration value of 1100 $\mu g/m^3$ was found; when this particular profile is not considered, the maximum concentration is 600 $\mu g/m^3$.

[d]On 14 May, in situ measurements during aircraft descent between 13:46 and 13:56 UTC yielded a 5.5 g/m^2 column loading and a 4700 $\mu g/m^3$ peak concentration, but there is some evidence of ice or ice coatings leading to an overestimate during that profile (Johnson et al., submitted manuscript, 2011); when these 10 minutes of data are omitted, in situ column loads of 0.1–0.7 g/m^2 and a maximum concentration of 1400 $\mu g/m^3$ are observed.

Falcon 20E aircraft. In that paper, volcanic ash layers with a depth of 0.1–3 km and horizontal extent 100–300 km are described to have been observed by lidar at altitudes 1–7 km; the geometrical parameters of the ash layers were thus were thus quite similar to those observed with our FAAM BAe-146 aircraft. The lidar operated at a wavelength of 2 μm, and its use was limited to ash detection, whereas concentration was inferred from their in situ size-distributions. On 17 May, the Falcon aircraft flew over the North Sea just 135 km to the Southeast of where we observed a concentration of 800 $\mu g/m^3$, and 1.5 hours later. From the advection of the ash plume on the satellite imagery, we can state that nearly (but not exactly) the same air mass was sampled. Their article reports typical (maximum) concentrations of 190 (540) $\mu g/m^3$, and layers located in the 3.3–6.5 km altitude range on that flight; our results are comparable to theirs (see Table 3), although their concentrations are ~40% smaller (this difference being within our factor of two uncertainty). A detailed comparison between of the FAAM BAe-146 data set and the Falcon 20E data set on that day is made by Turnbull et al. (submitted manuscript, 2011).

[27] Figure 4 displays the maps of the volcanic ash column loadings estimated from the lidar, overlaid on satellite "dust RGB" images obtained from the Spinning Enhanced Visible and Infrared Imager (SEVIRI) on Meteosat Second Generation (MSG) taken around mid-flight. The information that can be extracted from this type of image is qualitative, and volcanic ash is detected in a luminous orange-pink color in the current combination of layer height and optical properties. Not surprisingly, the lidar data indicate a large spatial coherence with the satellite images for the days with a larger ash load (14–17 May), whereas no ash is discernible in the 4–5 May satellite images. By visual comparison between the two products, we infer that ash detection in the SEVIRI "dust RGB" product is sensitive to column loadings corresponding to lidar estimates above roughly ~0.2 g/m^2 during our observations. Prior to the Eyjafjallajökull eruption, the London VAAC exploited only qualitative indices from satellite imagery; the latest research by Francis et al. (submitted manuscript, 2011) goes into the direction of exploiting the SEVIRI channels for quantitative retrievals.

[28] Figure 5 displays maps of the volcanic ash columnar peak concentration estimated from the lidar, overlaid on predicted peak ash concentration fields obtained using the atmospheric dispersion model NAME. The model fields are for the FL000–FL200 vertical range, where in the aviation sector FL (flight level) indicates a pressure level, corresponding to a nominal altitude in hundreds of feet computed for a standard atmosphere; the vertical range in Figure 5 is thus approximately equivalent to 0–6 km above sea level. The model fields shown here are from post-event re-runs, and differ from the ash dispersion forecasts released during the event in that analysis meteorological fields have been used, rather than forecast. On 4 May the predicted location and peak concentrations agree well with the observations. On 5 May the observed ash plume is found ~250 km further East than modeled, covering the whole of Great Britain rather than just its Western half. On 14 May, we observe large concentrations from the Midlands to the Outer Hebrides, whereas the model places the plume some ~500 km to the Northwest. Devenish et al. (submitted manuscript, 2011) and Webster et al. (submitted manuscript, 2011) show that the location of the predicted plume over the United Kingdom on this day was very sensitive to uncertainties in the source

Table 4. Per-Flight Estimate of Plume Along-Track Horizontal Extent in km at Three Different Altitude Ranges for the Major Ash Features Observed[a]

Date	Layer Altitude Range		
	2–3.5 km	3.5–5.5 km	5.5–8 km
4 May	180	85, 150	—
5 May	330	175	—
14 May	—	—	550
16 May	—	500 (75)	—
17 May[b]	500 (85)	500 (85)	500 (85)
18 May	150	120	—

[a]The number in parentheses denotes the along-track extent of the feature with concentration >500 $\mu g/m^3$.

[b]On 17 May a sloping feature was observed when flying along the 54N parallel: the plume started at low altitude and low column load over England, and both the plume height and its column load increased substantially over the North Sea.

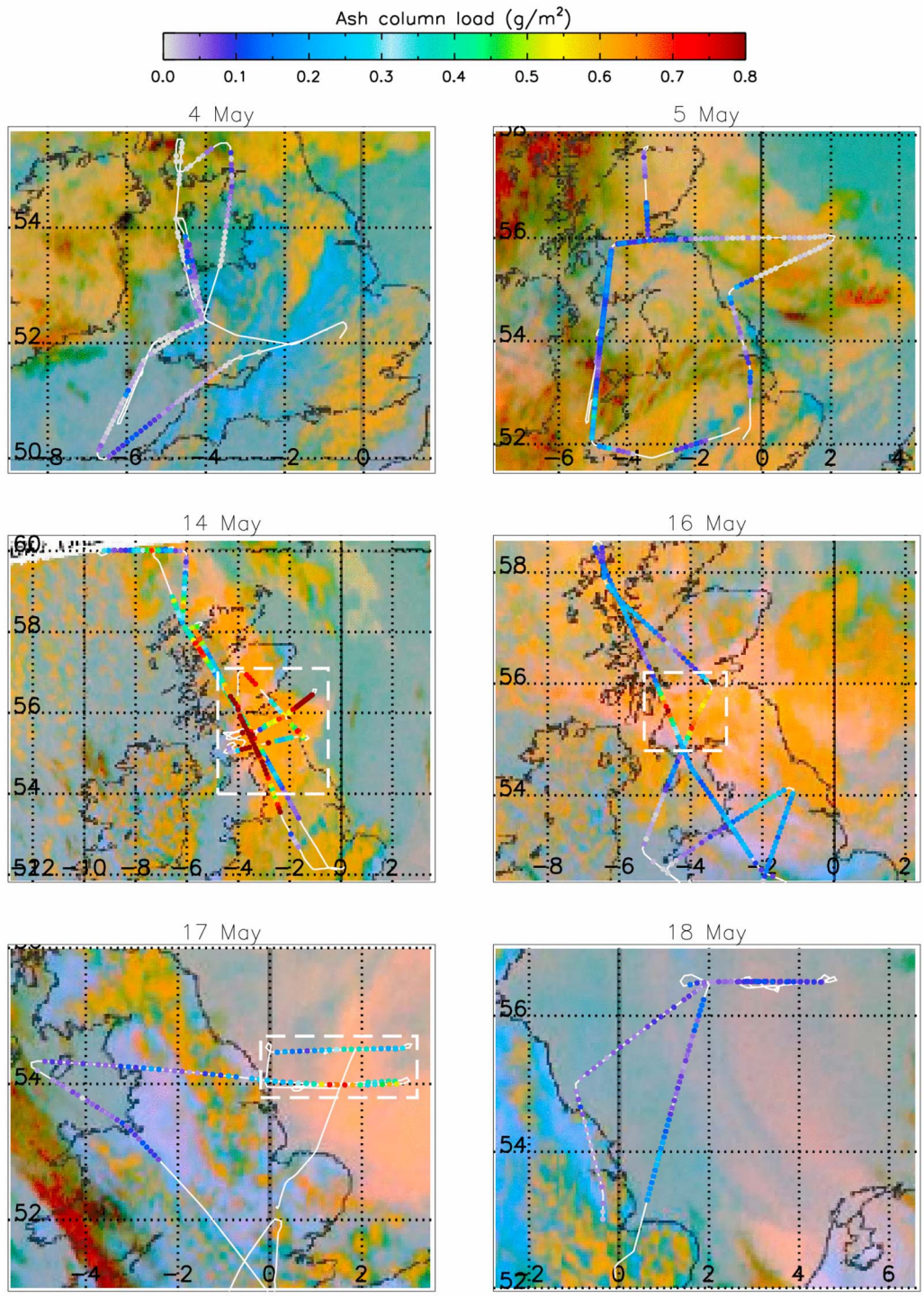

Figure 4. Maps of volcanic ash column load, estimated with the lidar, overlaid on "dust RGB" images derived from SEVIRI. The satellite images are for the following times: 13:00 (4 May), 12:00 (5 May), 15:00 (14 May), 15:00 (16 May), 16:00 (17 May), and 13:00 (18 May). The white dashed lines indicate regions of larger ash content, selected for statistical analysis.

eruption parameters. On 16 May, the model predicts concentrations greater than 200 μg/m^3 over most of Great Britain and Ireland, whereas our observations and the satellite imagery suggest that the volcanic ash mainly affects locations Northeast of a line joining the Isle of Man to Birmingham. On 17 May, we observe a concentration of 800 μg/m^3 at 54°N, 1.7°E over the North Sea, whereas for the model that same spot corresponds to a predicted concentration less than 200 μg/m^3. Finally, on 18 May the NAME predicted peak ash concentrations are larger than the observations suggest. In general, our observations seem to confirm the magnitude of the ash concentrations

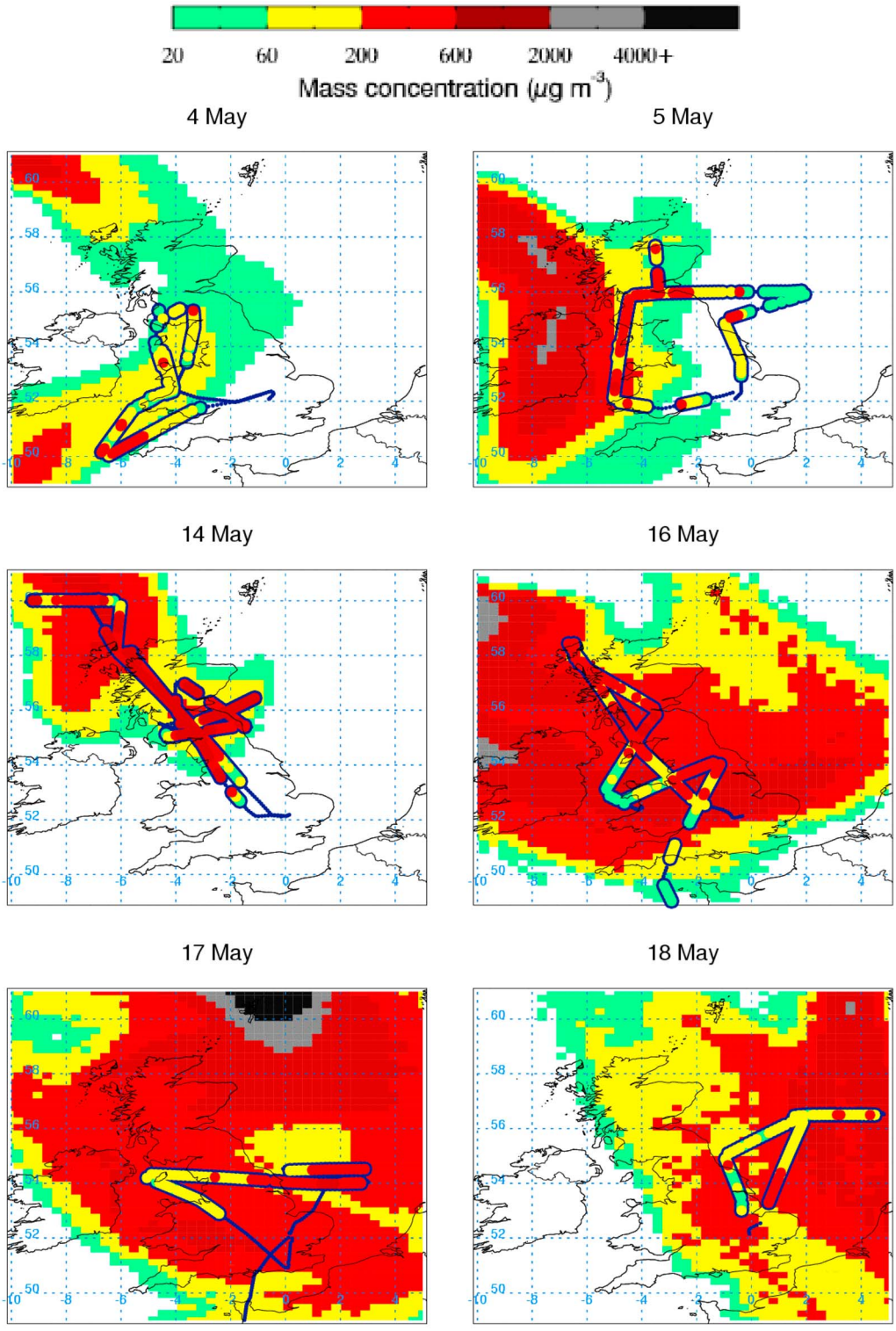

Figure 5. Maps of volcanic ash columnar peak concentration, estimated with the lidar, overlaid on predicted peak ash concentration fields derived from NAME dispersion model re-runs for FL000–FL200 (approximately 0–6 km height range) and for the 12:00–18:00 UTC time range. The same nonlinear color scale applies to the aircraft lidar observations and NAME modeled data sets.

derived from the model, but with scatter in some cases ascribed to positional errors in the plume. More detailed assessments of model performance against our airborne observations are to be found in work by Grant et al. (manuscript in preparation, 2011), Webster et al. (submitted manuscript, 2011), Kristiansen et al. (submitted manuscript, 2011), and Devenish et al. (submitted manuscript, 2011).

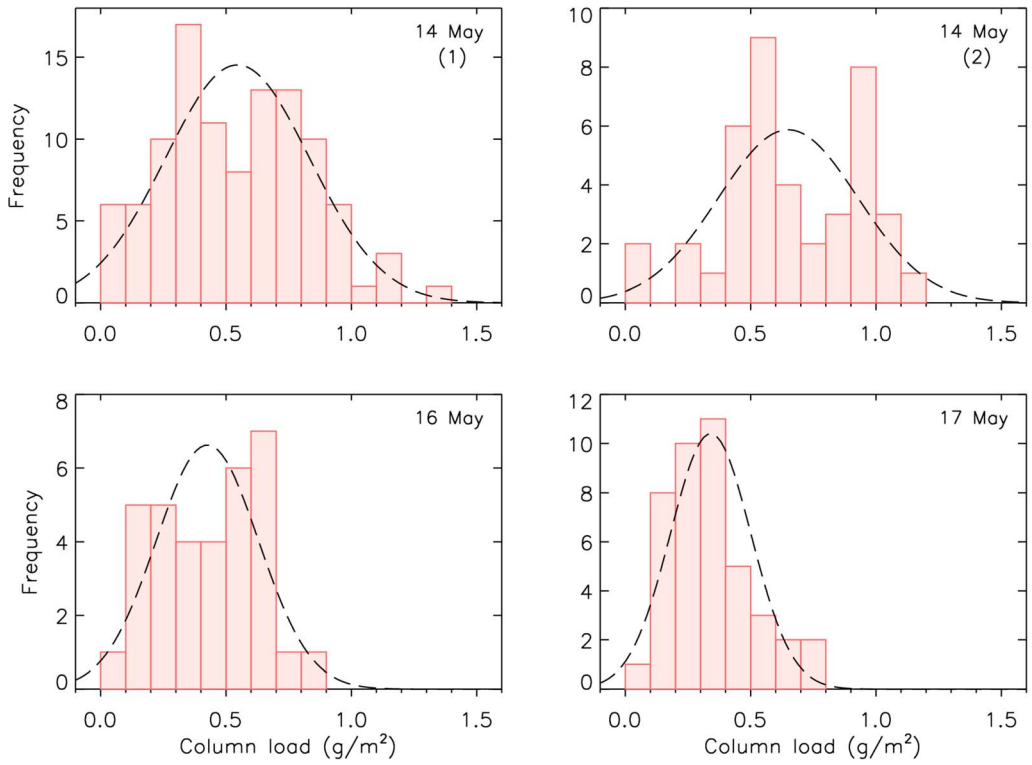

Figure 6. Distribution of aircraft lidar observations of volcanic ash column load within the regions denoted in Figure 4 by a dashed white line and summarized in Table 5. A Gaussian curve with the mean and standard deviation of the data set is superimposed (dashed line).

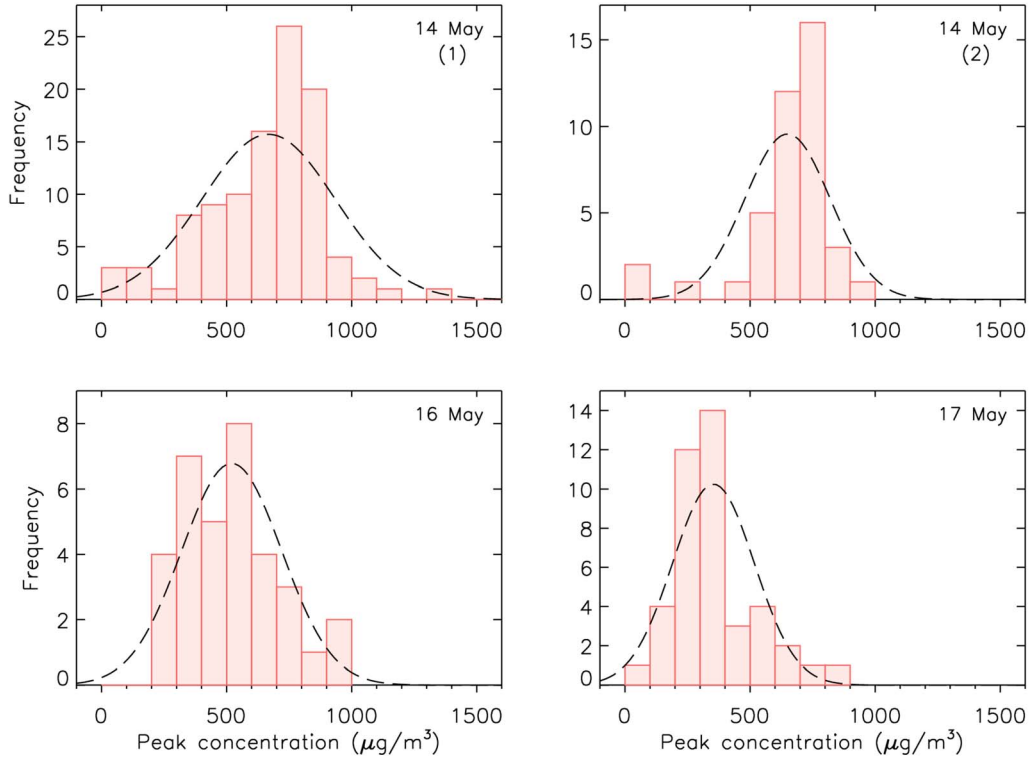

Figure 7. Distribution of aircraft lidar observations of volcanic ash columnar peak concentration within the regions denoted in Figure 4 by a dashed white line and summarized in Table 5. A Gaussian curve with the mean and standard deviation of the data set is superimposed (dashed line).

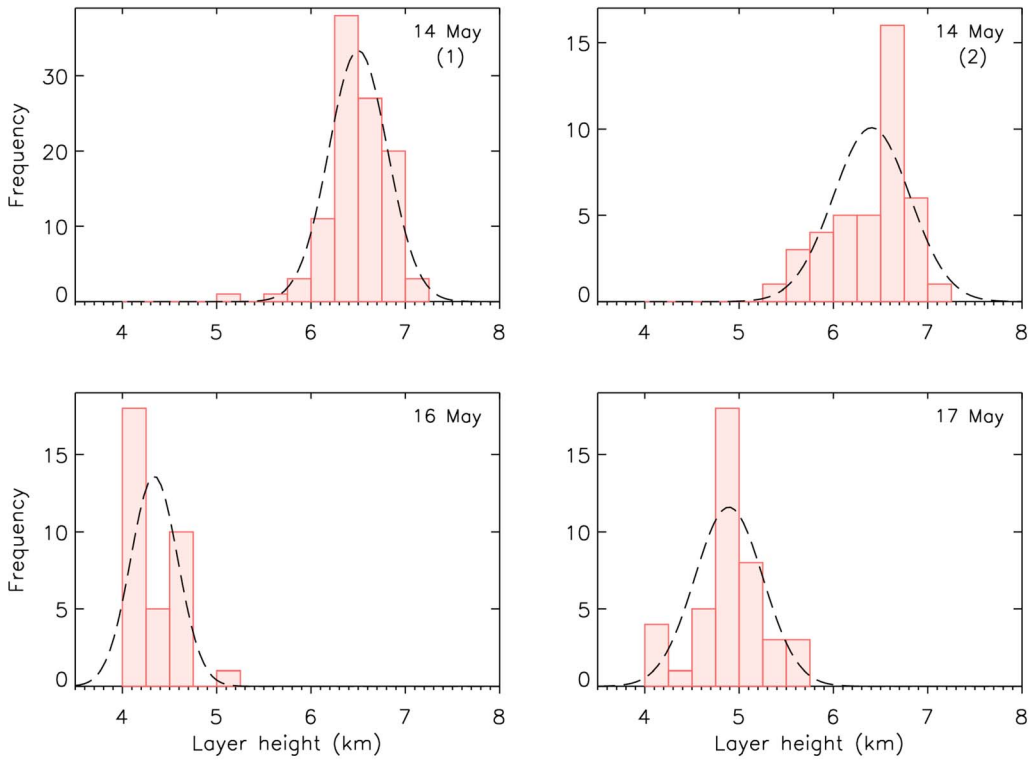

Figure 8. Distribution of aircraft lidar observations of volcanic ash layer height within the regions denoted in Figure 4 by a dashed white line and summarized in Table 5. A Gaussian curve with the mean and standard deviation of the data set is superimposed (dashed line). See text for our definition of layer height.

[29] Regions of larger ash content have been selected for the 14, 16 and 17 May flights, and are shown in Figure 4 (dashed white line), with reference to the lidar data. Our data within these regions might be of a particular interest for a comparison/validation of satellite retrieval schemes; we therefore use them for assessing the variability of the ash spatial distribution. This variability is of importance also when attempting to characterize the performance of atmospheric dispersion models such as NAME. We have performed a more detailed statistical analysis on the profiles enclosed in the selected region, and the results are displayed in Figures 6–8 and summarized in Table 5. Ash column loads in these larger ash content regions spanned 0–1.3 g/m^2, and averages of this same quantity were between 0.34 and 0.65 g/m^2; maxima within each region were of the order of the double of the observed average. Ash column load distributions tend to show two maxima, owing to the patchy nature of the layers.

[30] Peak concentrations in the larger ash content regions spanned 0–1900 μg/m^3 and averages spanned 350–670 μg/m^3; as for column loads, maximum concentration within each region were of the order of the double of the means, except for the 14 May (1) case where the maximum reached three times the average. Distributions of layer height in the larger ash content regions were relatively narrow, and for this reason in Table 5 we only give the mean for each case; standard deviations are 0.3–0.4 km, whereas the layer height distribution extremes extend ±0.5–1 km from the mean; averages of layer depths are consistently 1.1–1.4 km.

6. Conclusions

[31] Airborne observations of volcanic ash have been performed during the eruption of Eyjafjallajökull with an elastic backscatter lidar and in situ probes, and the airborne lidar has proven a powerful tool for mapping ash layers in

Table 5. Statistical Parameters of the Distribution of Volcanic Ash Column Loadings, Columnar Peak Concentrations and Layer Heights for the Larger Ash Content Regions Outlined With a White Dashed Line in Figure 4[a]

			Column Load (g/m^2)			Peak Concentration (μg/m^3)		
Date	Time (UTC)	Layer Height (km)	Mean	Median	SD	Mean	Median	SD
14 May (1)	10:35–15:20	6.5	0.55	0.57	0.29	670	710	270
14 May (2)	17:45–18:40	6.4	0.65	0.62	0.28	650	700	170
16 May	13:50–15:35	4.3	0.43	0.44	0.20	520	510	200
17 May	14:15–16:05	4.9	0.34	0.34	0.16	350	320	160

[a]On 14 May a double flight was performed; the analysis has been split accordingly. Layer depth 1.1–1.4 km. SD, standard deviation.

three dimensions. The ability to vertically profile the atmosphere yields an advantage over passive sensors in that the vertical structure of the layers is resolved, and that the observed signal is not sensitive to parameters such as ash layer temperature and ground reflection or emission. Moreover, when compared to in situ sampling techniques, it permits to sample the whole atmospheric column, and thus to fly in an ash-free area above the layers. When used in combination, lidar and in situ sampling of the particle size-distribution yield and invaluable combination of complementary data.

[32] The size-distributions (Johnson et al., submitted manuscript, 2011) were used to derive, for each of six research flights, the quantities needed to convert aerosol extinction coefficient, as derived from the lidar measurements, to ash mass concentration: coarse extinction fraction (ranging 0.5–1) and specific extinction (0.6–0.9 m^2/g). This is a conversion that leads to an uncertainty estimated around a factor of two, but on the other hand leads to the estimate of concentration fields, which are a useful product. Most existing estimates of the concentration of airborne volcanic ash are based on optical measurements and are thus prone to similar conversion errors [see, e.g., *Harrison et al.*, 2010; *Schumann et al.*, 2011; *Gasteiger et al.*, 2011; *Marenco and Hogan*, 2011; Hogan et al., manuscript in preparation, 2011]. As data of airborne volcanic ash concentrations are rather limited, such an uncertainty is deemed acceptable, and the lidar data set is considered invaluable for comparisons with NAME model predictions, which as mentioned earlier in this paper are also affected by significative uncertainties, due to an incomplete knowledge of the source and other important parameters. The estimates of the volcanic ash specific extinction have to be compared to the results given in other works. At the moment, existing estimates of the specific extinction for volcanic ash are as follows: 0.5 m^2/g [*Ansmann et al.*, 2010]; 0.4–1.2 m^2/g [*Gasteiger et al.*, 2011]; 0.64 m^2/g [*Ansmann et al.*, 2011]; and 0.8 m^2/g (Hogan et al., manuscript in preparation, 2011). As these have been derived with differing assumptions and methodologies (including different values for the density) we can state that a reasonable agreement exists.

[33] During our six research flights, lidar-derived aerosol extinction coefficients of up to 1.2 km^{-1} and AOD of up to 0.85 were observed, corresponding to estimated ash concentrations of up to 1900 $\mu g/m^3$ and column loadings of up to 1.3 g/m^2. Ash layers extended 85–550 km in the horizontal along-track direction and were found to consist of thin layers 0.5–3 km deep, located at altitudes 2–8 km above sea level. By combining the typical concentration encountered on each flight with the maximum horizontal extent of the ash patches, we estimate that an aircraft flying at constant level through the extent of the plume could have experienced integrated ash doses of the order of 20 g/m^2 on 4 and 18 May up to 360 g/m^2 on 14 May, with intermediate values ranging 100–150 g/m^2 on the other days. We observed spatial and temporal variability of the ash layers to occur on a wide range of scales, sometimes as small as tens of kilometers in the horizontal and 500 m in the vertical: this makes the relationship between peak concentrations and the likely exposure on a given flight path difficult to predict. At the state of the art, we cannot expect NAME to accurately represent features on the smaller scales, given the resolution of the driving meteorology, the parametrization of sub-scale processes, and the coarse representation of the source.

[34] A rudimentary comparison with areas that the SEVIRI "dust RGB" satellite imagery highlights with the typical orange-pink color showed the consistency of the two data sets for column loads above ~0.2 g/m^2. A comparison with NAME predicted ash concentrations showed a general agreement on the magnitude of peak ash concentrations, but with some scatter ascribed to positional errors in some cases. More detailed comparisons have been conducted, with NAME [*Dacre et al.*, 2011; *Devenish et al.*, 2011; Grant et al., manuscript in preparation, 2011; Webster et al., submitted manuscript, 2011; Devenish et al., submitted manuscript, 2011] and with remote sensing products (Newman et al., submitted manuscript, 2011). The latter paper also validates the lidar extinction profiles and the in situ size-distributions used here, by performing a radiative closure which matches well with upwelling radiation measurements in both the visible and infrared.

[35] **Acknowledgments.** Airborne data was obtained using the BAe-146-301 Atmospheric Research Aircraft (ARA) flown by Directflight Ltd. and managed by the Facility for Airborne Atmospheric Measurements (FAAM), which a joint entity of the Natural Environment Research Council (NERC) and the Met Office. The staff of the Met Office, FAAM, Direct Flight, Avalon Engineering and BAE Systems are thanked for their dedication in making the present measurement campaign a success. We also thank Eumetsat for providing the "dust RGB" product.

References

Allen, A. G., T. A. Mather, A. J. S. McGonigle, A. Aiuppa, P. Delmelle, B. Davison, N. Bobrowski, C. Oppenheimer, D. M. Pyle, and S. Inguaggiato (2006), Sources, size distribution and downwind grounding of aerosols from Mount Etna, *J. Geophys. Res.*, *111*, D10302, doi:10.1029/2005JD006015.

Ansmann, A., et al. (2010), The 16 April 2010 major volcanic ash plume over central Europe: EARLINET lidar and AERONET photometer observations at Leipzig and Munich, Germany, *Geophys. Res. Lett.*, *37*, L13810, doi:10.1029/2010GL043809.

Ansmann, A., et al. (2011), Ash and fine-mode particle mass profiles from EARLINET-AERONET observations over central Europe after the eruptions of the Eyjafjallajökull volcano in 2010, *J. Geophys. Res.*, *116*, D00U02, doi:10.1029/2010JD015567.

Balkanski, Y., M. Schulz, T. Claquin, and S. Guibert (2007), Reevaluation of mineral aerosol radiative forcings suggests a better agreement with satellite and AERONET data, *Atmos. Chem. Phys.*, *7*, 81–95.

Bingemer, H., et al. (2011), Atmospheric ice nuclei in the Eyjafjallajökull volcanic ash plume, *Atmos. Chem. Phys. Discuss.*, *11*, 2733–2748.

Bukowiecki, N., et al. (2011), Ground-based and airborne in-situ measurements of the Eyjafjallajökull volcanic aerosol plume in Switzerland in spring 2010, *Atmos. Chem. Phys. Discuss.*, *11*, 12,949–13,002.

Carn, S. A., et al. (2011), In situ measurements of tropospheric volcanic plumes in Ecuador and Colombia during TC^4, *J. Geophys. Res.*, *116*, D00J24, doi:10.1029/2010JD014718.

Clarisse, L., F. Prata, J.-L. Lacour, D. Hurtmans, C. Clerbaux, and P.-F. Coheur (2010), A correlation method for volcanic ash detection using hyperspectral infrared measurements, *Geophys. Res. Lett.*, *37*, L19806, doi:10.1029/2010GL044828.

Dacre, H. F., et al. (2011), Evaluating the structure and magnitude of the ash plume during the initial phase of the 2010 Eyjafjallajökull eruption using lidar observations and NAME simulations, *J. Geophys. Res.*, *116*, D00U03, doi:10.1029/2011JD015608.

DeSouza-Machado, S. G., L. L. Strow, S. E. Hannon, and H. E. Motteler (2006), Infrared dust spectral signatures from AIRS, *Geophys. Res. Lett.*, *33*, L03801, doi:10.1029/2005GL024364.

Devenish, B. J., D. J. Thomson, F. Marenco, S. J. Leadbetter, H. Ricketts, and H. F. Dacre (2011), A study of the arrival over the United Kingdom in April 2010 of the Eyjafjallajökull ash cloud using ground-based lidar and numerical simulations, *Atmos. Environ.*, doi:10.1016/j.atmosenv.2011.06.033, in press.

Di Girolamo, P., M. Cacciani, A. D. Sarra, G. Fiocco, and D. Fuà (1994), Lidar observations of the Pinatubo aerosol layer at Thule, Greenland, *Geophys. Res. Lett.*, *21*, 1295–1298.

Durant, A. J., R. A. Shaw, W. I. Rose, Y. Mi, and G. G. J. Ernst (2008), Ice nucleation and overseeding of ice in volcanic clouds, *J. Geophys. Res.*, *113*, D09206, doi:10.1029/2007JD009064.

European Union (2010), European measures to minimise disruption caused by volcanic ash, *Press Release IP/10/601*, Brussels, 21 May.

Fernald, F. G. (1984), Analysis of atmospheric lidar observations: Some comments, *Appl. Opt.*, *23*, 652–653.

Flentje, H., H. Claude, T. Elste, S. Gilge, U. Köhler, C. Plass-Dülmer, W. Steinbrecht, W. Thomas, A. Werner, and W. Fricke (2010), The Eyiafjallajökull eruption in April 2010—Detection of volcanic plume using in-situ measurements, ozone sondes and lidar-ceilometer profiles, *Atmos. Chem. Phys.*, *10*, 10,085–10,092.

Freudenthaler, V., et al. (2009), Depolarization ratio profiling at several wavelengths in pure Saharan dust during SAMUM 2006, *Tellus, Ser. B*, *61*, 165–179.

Gangale, G., A. J. Prata, and L. Clarisse (2010), The infrared spectral signature of volcanic ash determined from high-spectral resolution satellite measurements, *Remote Sens. Environ.*, *114*, 414–425.

Gasteiger, J., S. Groß, V. Freudenthaler, and M. Wiegner (2011), Volcanic ash from Iceland over Munich: Mass concentration retrieved from ground-based remote sensing measurements, *Atmos. Chem. Phys.*, *11*, 2209–2223.

Gauthier, P.-J., and M.-F. Le Cloarec (1998), Variability of alkali and heavy metal fluxes released by Mt. Etna volcano, Sicily, between 1991 and 1995, *J. Volcanol. Geotherm. Res.*, *81*, 311–326.

Gertisser, R. (2010), Eyjafjallajökull volcano causes widespread disruption to European air traffic, *Geol. Today*, *26*, 94–95.

Guffanti, M., D. J. Schneider, K. L. Wallace, T. Hall, D. R. Bensimon, and L. J. Salinas (2010), Aviation response to a widely dispersed volcanic ash and gas cloud from the August 2008 eruption of Kasatochi, Alaska, USA, *J. Geophys. Res.*, *115*, D00L19, doi:10.1029/2010JD013868.

Harrison, R. G., K. A. Nicoll, Z. Ulanowski, and T. A. Mather (2010), Self-charging of the Eyjafjallajökull volcanic ash plume, *Environ. Res. Lett.*, *5*, 024004, doi:10.1088/1748-9326/5/2/024004.

Hobbs, P. V., L. F. Radke, J. H. Lyons, R. J. Ferek, and D. J. Coffman (1991), Airborne measurements of particles and gas emissions from the 1990 volcanic eruptions of Mount Redoubt, *J. Geophys. Res.*, *96*, 18,735–18,752.

Hoffmann, A., C. Ritter, M. Stock, M. Maturilli, S. Eckhardt, A. Herber, and R. Neuber (2010), Lidar measurements of the Kasatochi aerosol plume in August and September 2008 in Ny-Ålesund, Spitzbergen, *J. Geophys. Res.*, *115*, D00L12, doi:10.1029/2009JD013039.

Hunton, D. E., et al. (2005), In-situ aircraft observations of the 2000 Mt. Hekla volcanic cloud: Composition and chemical evolution in the Arctic lower stratosphere, *J. Volcanol. Geotherm. Res.*, *145*, 23–34.

Ilyinskaya, E., V. I. Tsanev, R. S. Martin, C. Oppenheimer, J. Le Bond, G. M. Sawyer, and M. T. Gudmundsson (2011), Near-source observations of aerosol size distributions in the eruptive plumes from Eyjafjallajökull volcano, March–April 2010, *Atmos. Environ.*, *45*, 3210–3216.

International Civil Aviation Organization (2010), Volcanic ash contingency plan EUR and NAT regions, *EUR Doc 019*, 2nd ed., Paris.

Jones, A., D. Thomson, M. Hort, and B. Devenish (2007), The UK Met Office's next-generation atmospheric dispersion model, NAME III, in *Air Pollution Modelling and Its Application XVII*, edited by C. Borrego and A.-L. Norman, pp. 580–589, Springer, Dordrecht, Netherlands.

Klett, J. D. (1985), Lidar inversion with variable backscatter/extinction ratios, *Appl. Opt.*, *24*, 1638–1643.

Marenco, F., and R. Hogan (2011), Determining the contribution of volcanic ash and boundary-layer aerosol in backscatter lidar returns: A three-component atmosphere approach, *J. Geophys. Res.*, doi:10.1029/2010JD015415, in press.

Mona, L., A. Amodeo, A. Boselli, C. Cornacchia, G. D'Amico, A. Giunta, F. Madonna, and G. Pappalardo (2010), Observations of the Eyjafjallajökull eruption's plume at Potenza EARLINET station, *Geophys. Res. Abs.*, *12*, EGU2010.

Mona, L., A. Amodeo, G. D'Amico, A. Giunta, F. Madonna, and G. Pappalardo (2011), Multi-wavelength Raman lidar observations of the Eyjafjallajökull volcanic cloud over Potenza, southern Italy, *Atmos. Chem. Phys. Discuss.*, *11*, 12,763–12,803.

Oppenheimer, C., et al. (2010), Atmospheric chemistry of an Antarctic volcanic plume, *J. Geophys. Res.*, *115*, D04303, doi:10.1029/2009JD011910.

Osborne, S. R., A. J. Baran, B. T. Johnson, J. M. Haywood, E. Hesse, and S. Newman (2011), Short-wave and long-wave radiative properties of Saharan dust aerosol, *Q. J. R. Meteorol. Soc., Part A*, *137*, 1149–1167 doi:10.1002/qj.771.

Pieri, D., C. Ma, J. J. Simpson, G. Hufford, T. Grindle, and C. Grove (2002), Analyses of in-situ airborne volcanic ash from the February 2000 eruption of Hekla volcano, Iceland, *Geophys. Res. Lett.*, *29*(16), 1772, doi:10.1029/2001GL013688.

Pietruczuk, A., J. W. Krzyścin, J. Jaroslawski, J. Podgórski, P. Sobolewski, and J. Wink (2010), Eyjafjallajökull volcano ash observed over Belsk (52°N, 21°E), Poland, in April 2010, *Int. J. Remote Sens.*, *31*, 3981–3986.

Prata, A. J., G. Gangale, L. Clarisse, and F. Karagulian (2010), Ash and sulfur dioxide in the 2008 eruptions of Okmok and Kasatochi: Insights from high spectral resolution satellite measurements, *J. Geophys. Res.*, *115*, D00L18, doi:10.1029/2009JD013556.

Rose, W. I., G. J. S. Bluth, D. J. Schneider, G. G. J. Ernst, C. M. Riley, L. J. Henderson, and R. G. McGimsey (2001), Observations of volcanic clouds in their first few days of atmospheric residence: The 1992 eruptions of Crater Peak, Mount Spurr, Alaska, *Geol. J.*, *109*, 677–694.

Rose, W. I., et al. (2006), Atmospheric chemistry of a 33–34 hour old volcanic cloud from Hekla volcano (Iceland): Insights from direct sampling and the application of chemical box modeling, *J. Geophys. Res.*, *111*, D20206, doi:10.1029/2005JD006872.

Schumann, U., et al. (2011), Airborne observations of the Eyjafjalla volcano ash cloud over Europe during air space closure in April and May 2010, *Atmos. Chem. Phys.*, *11*, 2245–2279.

Stohl, A., et al. (2011), Determination of time- and height-resolved volcanic ash emissions and their use for quantitative ash dispersion modeling: The 2010 Eyjafjallajökull eruption, *Atmos. Chem. Phys.*, *11*, 4333–4351.

Thomas, H. E., and I. M. Watson (2010), Observations of volcanic emissions from space: Current and future perspectives, *Nat. Hazards*, *54*, 323–354.

Van de Hulst, H. C. (1957), *Light Scattering by Small Particles*, John Wiley, New York.

Watson, I. M., and C. Oppenheimer (2001), Photometric observations of Mt. Etna's different aerosol plumes, *Atmos. Environ.*, *35*, 3561–3572.

Young, S. A. (1995), Analysis of lidar backscatter profiles in optically thin clouds, *Appl. Opt.*, *34*, 7019–7031.

Zerefos, C., P. Nastos, D. Balis, A. Papayannis, A. Kelepertsis, E. Kannelopoulou, D. Nikolakis, C. Eleftheratos, W. Thomas, and C. Varotsos (2006), A complex study of Etna's volcanic plume from ground-based, in situ and space-borne observations, *Int. J. Remote Sens.*, *27*, 1855–1864.

J. Haywood, B. Johnson, F. Marenco, S. Newman, and K. Turnbull, Observational Based Research, Met Office, Exeter EX1 3PB, UK. (+44-1392-885393, http://www.metoffice.gov.uk/research/people/franco-marenco)

H. Ricketts, Centre for Atmospheric Science, University of Manchester, Manchester M139PL, UK.

H. Webster, Atmospheric Dispersion, Met Office, Exeter EX1 3PB, UK.